







## Antiferromagnetic structure and magnetic properties of $\text{Dy}_2\text{O}_2\text{Te}$ : An isostructural analog of the rare-earth superconductors $R_2\text{O}_2\text{Bi}$

Juanjuan Liu <sup>1</sup>, Jiale Huang,<sup>1</sup> Jieming Sheng,<sup>2,3,4</sup> Jinchen Wang,<sup>1</sup> Feihao Pan,<sup>1</sup> Hongxia Zhang,<sup>1</sup> Daye Xu,<sup>1</sup> Jianfei Qin <sup>5</sup>,  
Lijie Hao,<sup>5</sup> Yuanhua Xia,<sup>6</sup> Hao Li <sup>6</sup>, Xin Tong,<sup>3,4</sup> Liusuo Wu <sup>2</sup>, Peng Cheng <sup>1,\*</sup> and Wei Bao <sup>7,8,†</sup>

<sup>1</sup>Laboratory for Neutron Scattering and Beijing Key Laboratory of Optoelectronic Functional Materials and MicroNanoDevices,  
Department of Physics, Renmin University of China, Beijing 100872, China

<sup>2</sup>Department of Physics, Southern University of Science and Technology, Shenzhen 518055, China

<sup>3</sup>Institute of High Energy Physics, Chinese Academy of Sciences (CAS), Beijing 100049, China

<sup>4</sup>Spallation Neutron Source Science Center (SNSSC), Dongguan 523803, China

<sup>5</sup>China Institute of Atomic Energy, PO Box 275-30, Beijing 102413, China

<sup>6</sup>Key Laboratory of Neutron Physics and Institute of Nuclear Physics and Chemistry,  
China Academy of Engineering Physics, Mianyang 621999, China

<sup>7</sup>Department of Physics, City University of Hong Kong, Kowloon, Hong Kong SAR

<sup>8</sup>Center for Neutron Scattering, City University of Hong Kong, Kowloon, Hong Kong SAR



(Received 24 June 2021; revised 18 March 2022; accepted 21 March 2022; published 18 April 2022)

The rare-earth compounds  $R_2\text{O}_2\text{Bi}$  ( $R = \text{Tb}, \text{Dy}, \text{Er}, \text{Lu}, \text{Y}$ ) are newly discovered superconductors in the vicinity of a rare-earth magnetic long-range order. In this work, we determine the magnetic order of the parent compound  $\text{Dy}_2\text{O}_2\text{Te}$  by neutron scattering as the  $A$ -type antiferromagnetic structure below the Néel temperature  $T_N = 9.7$  K. The large staggered magnetic moment  $9.4(1) \mu_B$  per Dy at  $T = 3.5$  K lies in the basal  $ab$  plane. In a magnetic field, anomalous magnetic properties including the bifurcation between zero-field- and field-cooling magnetization, a butterfly-shaped magnetic hysteresis, and slow magnetic relaxation emerge, which are related to the field-induced metamagnetic transitions in  $\text{Dy}_2\text{O}_2\text{Te}$ . Our experimental findings could stimulate further research on the relation between antiferromagnetism and superconductivity in these rare-earth compounds.

DOI: [10.1103/PhysRevB.105.134419](https://doi.org/10.1103/PhysRevB.105.134419)

### I. INTRODUCTION

The layered compounds of the  $\text{ThCr}_2\text{Si}_2$  structure have shown great variety of novel superconducting and magnetic properties. The famous examples include the first heavy-fermion superconductor  $\text{CeCu}_2\text{Si}_2$  discovered in 1979 [1] and subsequent isostructural heavy-fermion superconductors [2–5]. More recently in 2008 Fe-based superconductors  $\text{BaFe}_2\text{As}_2$ ,  $\text{CaFe}_2\text{As}_2$ , and  $\text{SrFe}_2\text{As}_2$  of the  $\text{ThCr}_2\text{Si}_2$  structure were discovered [6–10]. Differently from conventional superconductivity which is caused by the electron-phonon interaction as explained by the BCS theory, magnetism is generally believed to play a crucial role in the unconventional superconductivity of the heavy-fermion [11,12] and Fe-based [13–23] superconductors.

$R_2\text{O}_2X$  ( $R = \text{rare earth}; X = \text{Te}, \text{Bi}, \text{Sb}$ ) represents a large family of materials with the  $\text{ThCr}_2\text{Si}_2$  crystal structure [24–26], which is composed of alternating  $[\text{R}_2\text{O}_2]^{2+}$  and  $X^{2-}$  stacking layers with opposite charges, in analog to the  $[\text{Cr}_2\text{Si}_2]^{4-}$  and  $\text{Th}^{4+}$  layers. The crystal structure is also referred to as the anti- $\text{ThCr}_2\text{Si}_2$  type for the switched signs of charges in the two layers. These kinds of materials demonstrate numerous intriguing physical properties such as

the metal-insulator transition [27–29], charge density waves [30,31], and the Kondo effect [32]. Most interestingly,  $R_2\text{O}_2\text{Bi}$  with heavy rare-earth elements ( $R = \text{Tb}, \text{Dy}, \text{Er}, \text{Lu}, \text{Y}$ ) were recently discovered to be superconducting below  $\sim 2$  K via excess oxygen incorporation [33–35]. Remarkably,  $\text{Tb}_2\text{O}_2\text{Bi}$  and  $\text{Er}_2\text{O}_2\text{Bi}$  are found to become antiferromagnetic in a first-ordered transition when they become superconductor, exhibiting the coexistence of antiferromagnetism with superconductivity according to the measurements of resistivity and susceptibility [27,34–36].

There have existed numerous discussions on the superconducting properties and mechanism of  $R_2\text{O}_2\text{Bi}$ . For example, the superconductivity is considered as arising from the metallic Bi square nets and the unit cell tetragonality ( $c/a$ ) is suggested to be closely related to superconducting transition temperature  $T_c$  [35]. The superconducting Bi square nets are also associated with the possibilities of exploring topological superconductivity [34,37]. Theoretical calculations revealed suppression of the charge density wave instability in  $R_2\text{O}_2\text{Bi}$  due to large spin-orbit coupling, which may be associated with the emergence of superconductivity [30]. Additionally, some members of  $R_2\text{O}_2\text{Bi}$  can be considered as an alternating stacking of antiferromagnetic  $[\text{R}_2\text{O}_2]^{2+}$  layers and superconducting Bi layers. The long-range-ordered rare-earth antiferromagnetism in the  $[\text{R}_2\text{O}_2]^{2+}$  layer naturally generates scientific interest in its relations with the superconductivity in the Bi layer. A very recent study on  $\text{Er}_2\text{O}_2\text{Bi}$  suggested that there

\*Corresponding author: pcheng@ruc.edu.cn

†Corresponding author: weibao@cityu.edu.hk

may be a competition between superconductivity and anti-ferromagnetic order [36]. Therefore, this series of materials provides a new platform for investigating the interplay between antiferromagnetism and superconductivity.

Antiferromagnetic properties of  $R_2O_2X$  compounds, however, have not been studied in depth. Take  $Dy_2O_2Te$ , for instance; the only knowledge about its physical properties so far comes from an early Mössbauer study, which shows that  $Dy_2O_2Te$  is an antiferromagnet with  $T_N \sim 10$  K [38]. However the antiferromagnetic structure and detailed magnetic properties are still unknown. Since the Te and Bi series have identical  $[R_2O_2]^{2+}$  layers, but the higher  $T_N$  makes it easier for the former compounds to access the ordered phase, the determination of the magnetic structure and the investigation of magnetic properties of  $R_2O_2Te$  would provide fundamental information on this exciting family of rare-earth materials  $R_2O_2X$ . Besides, due to the large quantum number  $J$ , many Dy-based materials exhibit peculiar magnetic properties such as slow magnetic relaxation behavior. This behavior has been widely observed in the Dy-based complex in the research of single-molecule magnets or compounds with diluted Dy ions, which arise from the magnetic quantum tunneling effect and weak interactions between molecules [39–43]. The occurrence of slow magnetic behavior in a correlated Dy-based compound is very rare. A recent example is  $Dy_2Ti_2O_7$ ; its interesting slow magnetic relaxation is possibly due to the special spin-ice state and dipolar spin correlations [44,45]. It would also be interesting to explore whether this peculiar magnetic property would exist in  $Dy_2O_2X$  series.

In this paper, we report the investigations on  $Dy_2O_2Te$ . We find that  $Dy_2O_2Te$  orders antiferromagnetically below the Néel temperature  $T_N = 9.7$  K. A collinear  $A$ -type magnetic structure with moments lying in the basal  $ab$  plane is determined directly through powder neutron diffraction measurements. The magnetization measurements reveal that  $Dy_2O_2Te$  exhibits magnetic-field-induced slow magnetic relaxation. Possible mechanisms such as the phonon bottleneck effect will be discussed.

## II. EXPERIMENTAL METHODS

Polycrystalline samples of  $Dy_2O_2Te$  were synthesized by solid-state reaction of Dy granules and Te and  $Dy_2O_3$  powders in stoichiometric portions. These reagents were mixed, pressed into pellets, and heated in an evacuated quartz tube at 1073 K for 24 h. The products were then reground, pressed into pellets, and annealed at 1223 K for 20 h. X-ray diffraction refinement indicates that samples prepared in such a way, referred to as sample A in the remaining text, contain about 6%–8% weight fraction of unreacted  $Dy_2O_3$  as an impurity phase. By adding extra amount of Te ( $\sim 5\%$ ) to the synthesis reagents, it is found that phase-pure  $Dy_2O_2Te$  samples can be obtained, and they are referred to as sample B. The magnetization measurements reported in this paper used sample B, while the neutron diffraction experiments were performed on sample A.

Powder x-ray diffraction (XRD) patterns were collected from a Bruker D8 Advance x-ray diffractometer using  $Cu K_\alpha$  radiation. Magnetization measurements were carried out in the Quantum Design MPMS3 and PPMS-14T. The

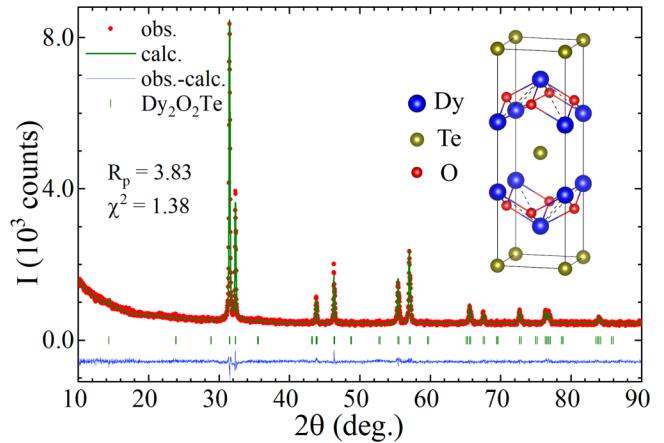


FIG. 1. The x-ray powder diffraction pattern of  $Dy_2O_2Te$  measured on sample B at room temperature. The inset shows the crystal structure of  $Dy_2O_2Te$ .

powder neutron diffraction experiments were carried out on the Xingzhi triple-axis spectrometer [46] at the China Advanced Research Reactor (CARR) and Xuanwu powder neutron diffraction spectrometer at China Academy of Engineering Physics (CAEP). Approximate 3.8 g of a  $Dy_2O_2Te$  powder sample sealed in a cylindrical vanadium or aluminium container was loaded into a closed cycle refrigerator that regulates the sample temperature from 3.5 K to 300 K. For neutron experiments on Xingzhi, a neutron velocity selector was used upstream to cleanly remove higher-order neutrons for the incident neutron energy fixed at 15 meV [46].

The program FULLPROF Suite [47] was used in the Rietveld refinement of neutron powder diffraction data. The aluminium peaks are accounted for by Le Bail fitting [48]. The BasIreps program of FULLPROF Suite is used for representation analysis to derive the possible magnetic structure modes. Because the dysprosium is highly neutron absorbing, the absorption correction was applied to neutron powder diffraction data.

## III. RESULTS AND DISCUSSION

### A. X-ray analysis and magnetic susceptibility

From the powder x-ray diffraction pattern and its Rietveld analysis shown in Fig. 1, sample B was confirmed to be phase-pure  $Dy_2O_2Te$ . Any possible impurities should be less than 1%.  $Dy_2O_2Te$  crystallizes in the tetragonal space group  $I4/mmm$ . The magnetic ions Dy occupy the Si sites of the  $ThCr_2Si_2$  structure. The lattice parameters obtained from the refinement are  $a = b = 3.925$  Å and  $c = 12.413$  Å. The nearest Dy-Dy distance is 3.536 Å which is indicated by the blue dashed line in Fig. 1.

The temperature-dependent magnetic susceptibility of  $Dy_2O_2Te$ , measured at  $H = 500$  Oe, is presented in Fig. 2. There is a cusp at  $T_N = 9.7$  K in the magnetization data indicating the occurrence of an antiferromagnetic transition. The susceptibility also exhibits an anomaly at about 30 K. At temperatures above 40 K, the linear relation between inverse magnetic susceptibility and temperature is apparent. Fitting the high-temperature data above 120 K to the Curie-Weiss law

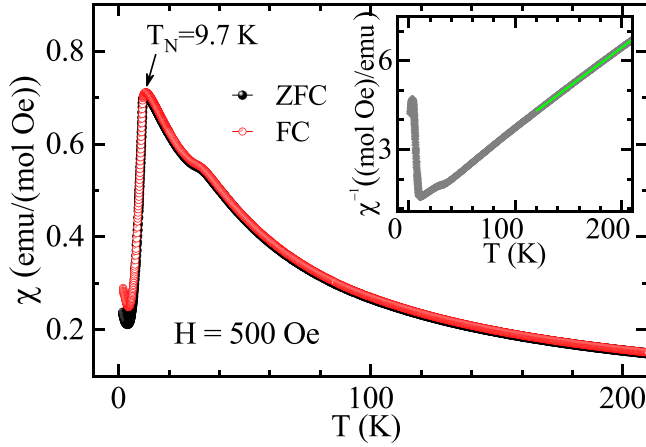


FIG. 2. Zero-field-cooling (ZFC) and field-cooling (FC) magnetic susceptibility of  $\text{Dy}_2\text{O}_2\text{Te}$  at  $H = 500$  Oe. The inverse magnetic susceptibility  $1/\chi$  versus temperature is plotted in the inset.

yields  $\mu_{\text{eff}} = 8.6 \mu_B$  and  $\theta_{CW} = -37.9$  K. The interpretation of the high-temperature fitting results needs to be careful in view of the crystal field scheme of the rare-earth ions in the material. We carried out the crystal field calculations based on the point-charge model using the software McPhase [49] for  $\text{Dy}_2\text{O}_2\text{Te}$ . The  $\text{Dy}^{3+}$  ion has a ground state of the 16-fold-degenerate  $J = 15/2$  ( $L = 5$ ,  $S = 5/2$ ) multiplet of an effective magnetic moment  $10.6 \mu_B$ . The multiplet is further split into eight doublets by the crystalline electrical field effect. The calculated first-excited crystal field levels are at 1.95 meV (23 K). Therefore in the high-temperature region of Fig. 2, the contributions from the excited states could be large and the Curie-Weiss fitting results for  $\mu_{\text{eff}}$  and  $\theta_{CW}$  do not represent the ground-state magnetic properties at the base temperature. The susceptibility anomaly around 30 K is likely caused by enhanced magnetic contributions from the thermal occupation of the 23 K crystal field levels. Indeed, evidence for the magnetic phase transition around 30 K has not been observed in our neutron diffraction experiments to be presented in the next part. The calculations based on the point-charge model are rough evaluations. However, the preliminary crystal field scheme is sufficient for an understanding of the magnetic susceptibility data.

Figure 3 shows the isothermal magnetization measurements for  $\text{Dy}_2\text{O}_2\text{Te}$  at various temperatures. With increasing applied magnetic field, two kinks are observed in  $M(H)$  at low temperatures. This behavior can be more clearly identified by two peaks at around 23 kOe and 43 kOe in the  $dM/dH$  curves as shown in inset (a) of Fig. 3. These two peaks gradually disappear with increasing temperature as illustrated by the contour plot of  $dM/dH$  in inset (b) of Fig. 3. Typically, these features are indications of metamagnetic transition [50], which will be further discussed in a following section. The magnetization approaches a saturated value  $6.9 \mu_B/\text{Dy}^{3+}$  at 14 T and those measurement temperatures. This value is quite close to 2/3 of the full saturation moment of  $\text{Dy}^{3+}$  at the ground state ( $\sim 10 \mu_B$ ), which agrees well with the expectation of powder-averaged magnetization of an easy-plane magnet. In our McPhase calculations on  $\text{Dy}_2\text{O}_2\text{Te}$ , the crystal field  $xyz$  axes are chosen to be along the crystal lattice  $abc$  directions.

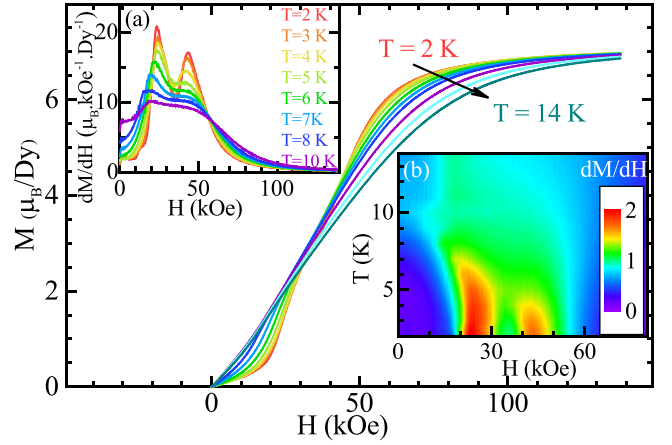


FIG. 3. Magnetization isotherms measured at the specified temperatures. Initially, the data were measured after zero-field-cooling the sample to 2 K and with increasing field. After the measurement at 2 K, the field was cooled to zero at this temperature, then warmed up directly to 3 K for next measurement, and so on. Insets: (a) The  $dM/dH$  curves at different temperatures. (b) Contour plot of  $dM/dH$  as a function of temperature and field.

Then the calculated ground-state wave functions are

$$E_{0\pm} = \pm 0.9601|\pm 1/2\rangle \pm 0.2529|\mp 7/2\rangle \pm 0.1198|\pm 9/2\rangle.$$

This result suggests that the magnetic moment along the  $c$  axis would be quite small and it should lie in the  $ab$  plane. The following determination of magnetic structure by neutron scattering also provides a consistent result.

In addition, we measured the resistivity of  $\text{Dy}_2\text{O}_2\text{Te}$  at around room temperature which is about  $6 \times 10^3 \Omega \text{ cm}$ . The resistivity increases quickly with decreasing temperature and the data below 240 K cannot be obtained due to the upper limit of the PPMS measurement. Thus  $\text{Dy}_2\text{O}_2\text{Te}$  is a semiconductor, the same as previously reported for other members of  $R_2\text{O}_2\text{Te}$  ( $R = \text{La}, \text{Sm}, \text{Gd}$ ) [51].

## B. Magnetic structure

To determine the antiferromagnetic structure of  $\text{Dy}_2\text{O}_2\text{Te}$  below  $T_N = 9.7$  K and to check the possible magnetic transition around 30 K, powder neutron diffraction measurements were performed at  $T = 3.5, 15, 50$  K and room temperature, respectively. The temperature-dependent magnetic scattering at the Bragg peaks (0,0,2), (1,0,1), and (1,1,2) is shown in Figs. 4(a)–4(c). The temperature dependence of the magnetic (1,0,1) peak intensity is shown in Fig. 5(a). The intensity increases abruptly below 10 K, consistent with the antiferromagnetic transition at the Néel temperature revealed by magnetic susceptibility (Fig. 2). No further magnetic transition around 30 K can be detected in our neutron diffraction study.

The integer Miller index of the magnetic Bragg peaks in Figs. 4(a)–4(c) indicates that the antiferromagnetic structure of the Néel state below  $T_N$  does not increase the crystalline unit cell and the magnetic propagation vector  $\mathbf{k} = (0, 0, 0)$ . For  $\text{Dy}_2\text{O}_2\text{Te}$ , the space group of the crystal structure is  $I4/mmm$ . For magnetic structures with  $\mathbf{k} = (0, 0, 0)$ , its little group, which is the same as the crystal point group  $4/mmm$ ,

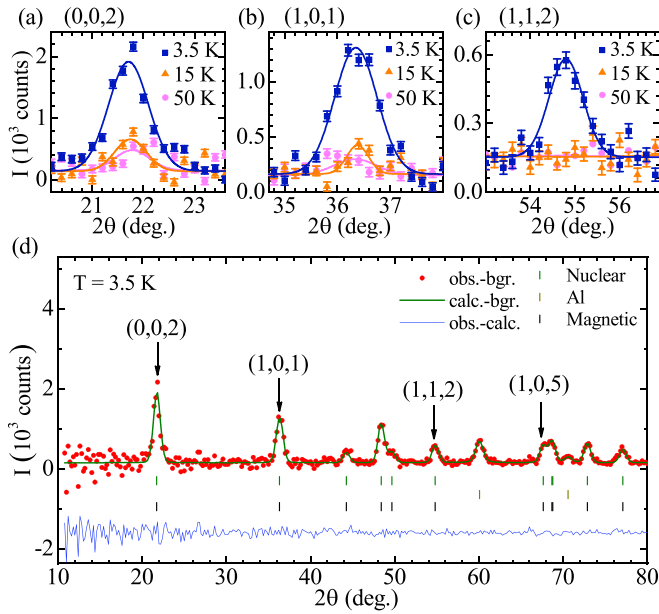


FIG. 4. (a)–(c) Neutron diffraction peak profiles for (0,0,2), (1,0,1), and (1,1,2) at selected temperatures. (d) The powder neutron diffraction pattern of  $\text{Dy}_2\text{O}_2\text{Te}$  at 3.5 K and the Rietveld refinement fit.

has ten irreducible representations (IRs), composed of eight one-dimensional IRs  $\Gamma_1 \cdots \Gamma_8$  and two two-dimensional IRs  $\Gamma_9$  and  $\Gamma_{10}$  according to the representation analysis [52]. The spin spaces for  $\text{Dy}^{3+}$  in the 4d site can be decomposed as

$$\Gamma = 1\Gamma_2 + 1\Gamma_7 + 1\Gamma_9 + 1\Gamma_{10}. \quad (1)$$

Among the four IRs of  $\Gamma_2$ ,  $\Gamma_7$ ,  $\Gamma_9$ , and  $\Gamma_{10}$ , the magnetic structure with  $\Gamma_9$  is the best fit with  $R_p = 3.55$ ,  $R_{wp} = 4.36$ , and  $\chi^2 = 3.44$  for the neutron powder diffraction pattern measured at 3.5 K [Fig. 4(d)]. The Dy neutron absorption correction has been included during the refinement, and an impurity phase of 5.6% in weight is identified in the neutron refinement, consistent with x-ray sample characterization. The resulting collinear A-type antiferromagnetic structure for  $\text{Dy}_2\text{O}_2\text{Te}$  is depicted in Fig. 5(b). The ordered moment per

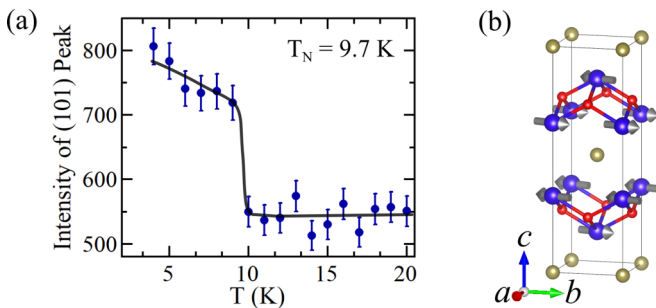


FIG. 5. (a) Temperature dependence of the peak intensity of (1,0,1) from neutron diffraction on  $\text{Dy}_2\text{O}_2\text{Te}$ . The solid line is a guide to the eye. (b) The antiferromagnetic structure of  $\text{Dy}_2\text{O}_2\text{Te}$  as determined by the Rietveld refinement of powder neutron diffraction data at  $T = 3.5$  K.

Dy ion obtained from Rietveld refinement is  $\mu = 9.4(1) \mu_B/\text{Dy}^{3+}$  at 3.5 K. With the tetragonal structure of  $\text{Dy}_2\text{O}_2\text{Te}$ , we can only conclude that the moments of the Dy ions are oriented within the  $ab$  plane in this powder diffraction investigation [53]. On the other hand, the calculations using the point-charge model by the McPhase program may provide a clue for the in-plane easy axis. Our calculations using the *singleion* module in McPhase indicate that the easy axis of  $\text{Dy}_2\text{O}_2\text{Te}$  could be the  $a$  axis or the crystallographically equivalent  $b$  axis.

The determination of magnetic structure provides important information in understanding the novel properties in the  $R_2\text{O}_2X$  ( $R = \text{rare earth}$ ;  $X = \text{Te, Bi, Sb}$ ) family of materials. The antiferromagnetic structure of  $\text{Dy}_2\text{O}_2\text{Te}$  shown in Fig. 5(b) reveals antiferromagnetic exchange coupling between the nearest-neighbor Dy ions and ferromagnetic exchange coupling between the next-nearest-neighbor Dy ions within the  $\text{Dy}_2\text{O}_2$  sublayer. The Te layer mediates another antiferromagnetic coupling between the neighboring  $\text{Dy}_2\text{O}_2$  sublayers. For superconducting  $\text{Dy}_2\text{O}_2\text{Bi}$  of the same crystal structure, magnetic transition disappears and superconducting transition emerges by excess oxygen incorporation as shown from the resistivity and susceptibility study [35]. Therefore the antiferromagnetic order of  $\text{Dy}_2\text{O}_2\text{Te}$  is possibly the competing order for the superconducting one in  $\text{Dy}_2\text{O}_2\text{Bi}$ . To verify this speculation, future studies may focus on how the antiferromagnetic order of semiconducting  $\text{Dy}_2\text{O}_2\text{Te}$  evolves through Bi doping to the superconductor, as in the heavy-fermion and Fe-based isostructural superconductors. Further investigations are also needed to check whether spin fluctuations exist in  $\text{Dy}_2\text{O}_2\text{Bi}$  with inelastic neutron scattering or the NMR techniques.

The material family of  $R_2\text{O}_2X$  contains many members of antiferromagnets and superconductors. In addition to the Dy series discussed above, we have also synthesized a  $\text{Tb}_2\text{O}_2\text{Te}$  sample and find that it undergoes an antiferromagnetic transition at  $T = 2.7$  K. According to previous reports [35,54], through Bi substitution for Te, superconductivity at around 2 K coexists with antiferromagnetism at  $T_N = 15$  K in  $\text{Tb}_2\text{O}_2\text{Bi}$ . A fertile field is indeed opened for systematic investigations of  $R_2\text{O}_2X$  compounds.

### C. Field-induced slow magnetic relaxation

The temperature dependence of magnetization at higher magnetic fields reveals further anomalous features. As shown in Fig. 6, the antiferromagnetic-like cusp gradually shifts to lower temperature with increasing field. The field-dependent cusp temperatures are plotted in Fig. 6(c) which marks the border between antiferromagnetic and paramagnetic states. The white points represent the maxima of  $dM/dH$  obtained in Fig. 3 and field-induced canted antiferromagnetic phases may exist in these regions. For  $H \leq 15$  kOe, the susceptibility in zero-field-cooling (ZFC) mode almost overlaps with that in field-cooling (FC) mode. However for  $H = 25$  kOe, a separation between ZFC and FC curves occurs below the antiferromagnetic transition temperature. For  $H \geq 30$  kOe, the bifurcation between the ZFC and FC magnetization becomes more obvious [Fig. 6(b)] and the cusp feature even disappears in the FC curve. Generally speaking, this behavior

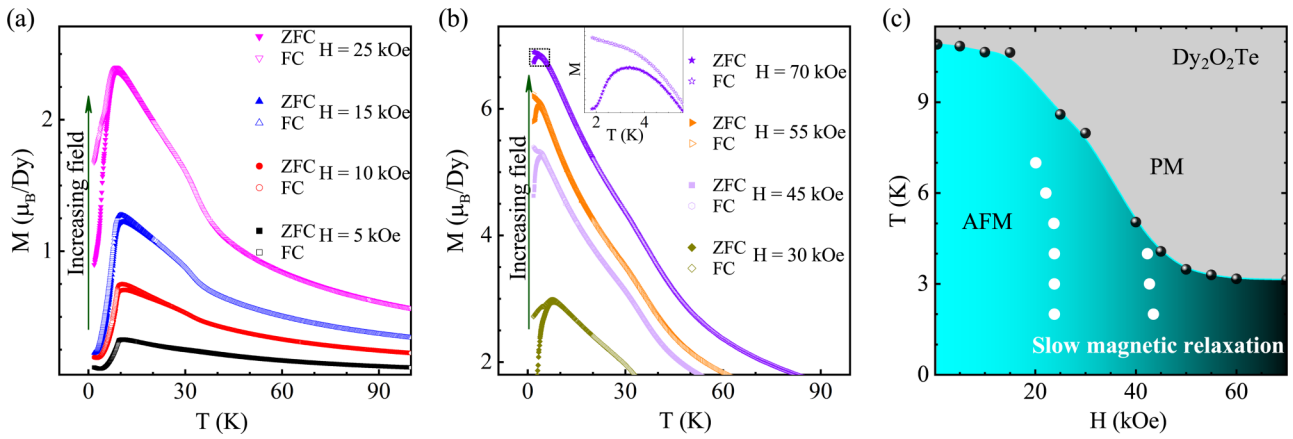


FIG. 6. (a) and (b) Magnetic susceptibility versus temperature of  $\text{Dy}_2\text{O}_2\text{Te}$  under different field. The solid and open symbols represent the results of ZFC and FC measurements, respectively. (c) The  $H$ - $T$  phase diagram of  $\text{Dy}_2\text{O}_2\text{Te}$ . The black spheres represent the cusp point of ZFC magnetic susceptibility. The white points represent the the maxima of  $dM/dH$  obtained in Fig. 3.

strongly resembles the spin frozen in spin-glass states [55,56]. Especially, the AC susceptibility measurement also tracks the peak of the real part of  $\chi'$  shifting to higher temperature with increasing frequency under a DC field of 40 kOe, while the peak of  $\chi'$  does not shift under zero DC field [illustrated by the arrow in Figs. 7(a) and 7(b)]. However, typical spin-glass

behavior could be easily suppressed by stronger magnetic field [55]; the bifurcations between the ZFC and FC susceptibilities, as well as the frequency-dependent peak temperature of  $\chi'$ , are actually induced and enhanced by magnetic field for  $\text{Dy}_2\text{O}_2\text{Te}$ . Therefore these phenomena may have a different origin.

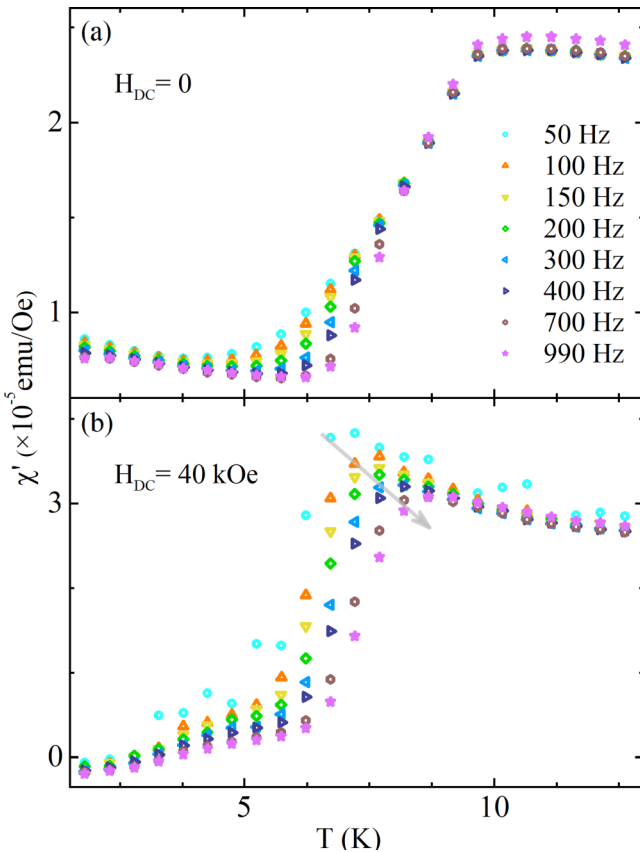


FIG. 7. (a) The temperature dependence of the real part of AC susceptibility  $\chi'$  under zero DC field and different frequencies. (b) Similar AC susceptibility measurements under DC field of 40 kOe.

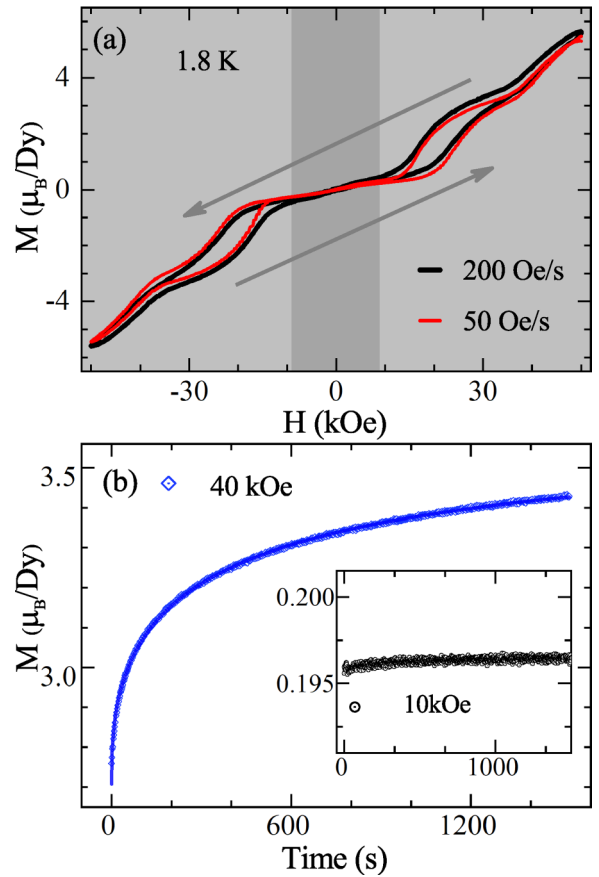


FIG. 8. (a) Hysteresis loops of  $\text{Dy}_2\text{O}_2\text{Te}$  at  $T = 1.8$  K measured with different field-sweeping rate. (b) Time dependence of magnetization when the magnetic field is fast settled to  $H = 40$  kOe at  $T = 1.8$  K. The inset shows similar measurement for  $H = 10$  kOe.

Figure 8(a) presents the hysteresis loop at  $T = 1.8$  K which has a butterfly shape. There are big differences between low- and high-field regions as well. Large magnetic hysteresis appears at  $H \geq 12$  kOe while it is absent at  $H \leq 12$  kOe. Furthermore, the loops measured under different field-sweeping rate do not overlap. The above observations strongly suggest the existence of magnetic-field-induced slow magnetic relaxation in  $\text{Dy}_2\text{O}_2\text{Te}$ . Therefore we directly measured the time-dependent magnetization under different field and temperature. As demonstrated in Fig. 8(b), at 1.8 K when the magnetic field is fast settled to  $H = 40$  kOe at  $T = 1.8$  K, the immediate measurement of sample susceptibility versus time reveals a slow relaxation. This slow magnetic relaxation behavior is obviously induced by higher magnetic field as it disappears in a similar measurement under  $H = 10$  kOe [inset of Fig. 8(b)].

The field-induced slow magnetic behaviors have been widely observed and investigated in single-molecule magnets [39–42] (many of them are Dy-based complexes) and inorganic compounds with diluted Dy ions [43]. They are explained as a result of the magnetic quantum tunneling (MQT) effect. The Dy ion has a very large  $J$ ; the Zeeman effect could bring different spin states to the same energy level and generate the MQT effect. When the actual field deviates from the tunneling field, the MQT needs to overcome energy barriers and has a low probability, and therefore will simultaneously generate slow magnetic relaxations. However this mechanism mainly applies in material with weak or absent interactions between Dy ions; it seems difficult to work for  $\text{Dy}_2\text{O}_2\text{Te}$  with long-range magnetic order, especially when the relaxation time is highly temperature dependent as shown in the following data, which contradicts the typical behavior of MQT. So other explanations are needed.

In order to get a quantitative analysis of the slow magnetic behavior, relaxation times  $\tau$  were extracted from least-squares fits of a stretched exponential equation to the relaxation curves [57]:

$$M(t) = M_0 - M_1 e^{-(\frac{t}{\tau})^\beta}. \quad (2)$$

In this equation,  $\tau$  and  $\beta$  are the fitting parameters. Since  $M(0) = M_0 - M_1$  and  $M(\infty) = M_0$ , then  $M_1/M_0$  can be defined as the ratio of the moments with slow relaxation to the total moments. The fitting results are presented in Figs. 9(a) and 9(b). At 1.8 K, the field-dependent relaxation time  $\tau$  has two maxima around 20 kOe and 38 kOe. The relaxation ratio  $M_1/M_0$  follows roughly the same field-dependent behavior, except the maxima slightly move toward higher field. At 5 K, both  $\tau$  and  $M_1/M_0$  are strongly reduced;  $M_1/M_0$  has a much weakened maximum at 20 kOe. If we compare this result with the magnetization isotherms in Fig. 3, one can easily find the close relations between the slow magnetic behaviors and two metamagnetic transitions. At 1.8 K, the maximum field for  $\tau$  and  $M_1/M_0$  is only slightly lower than the maximum field at which metamagnetic transitions emerge. With increasing temperature, the slow magnetic relaxations are suppressed similarly to that for metamagnetic transitions.

The two metamagnetic transitions are most likely spin-flip transitions from the antiferromagnetic ground state to

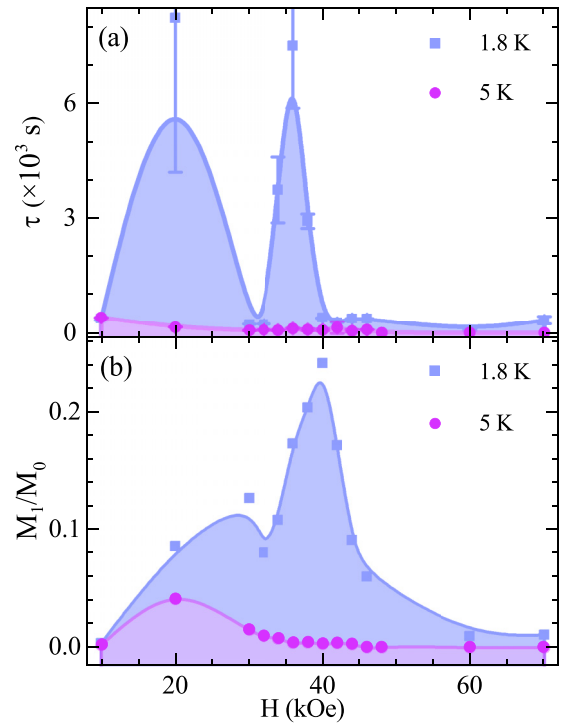


FIG. 9. Field- and temperature-dependent magnetic relaxation time  $\tau$  (a) and relaxation ratio  $M_1/M_0$  (b). The data were obtained by fitting the time-dependent magnetization as described in the text.

field-induced canted magnetic states. The above data and analysis strongly suggest the slow magnetic relaxations are actually induced by the transitions from different field-induced magnetic structures. A possible physical origin of this behavior is the phonon bottleneck effect [58–60]. This effect is due to the inefficient exchange between the spins and the thermal bath mediated by low-frequency phonons, resulting in slowing of the relaxation process. There have been reports about the phonon bottleneck effect leading to observation of magnetic quantum tunneling, slow magnetic relaxation, and butterfly-shaped hysteresis loops [58], but mainly in molecular complexes. On the other hand, it would also be interesting to check whether this slow magnetic behavior is associated with the possible formation, pinning, and movement of new magnetic domains [61]. Overall, this anomalous field-induced slow magnetic behavior has been rarely reported in inorganic correlated compounds. It would be worthwhile to further investigate its mechanism and whether these properties can be utilized to design novel magnetic devices.

#### IV. CONCLUSIONS

In summary, the anti- $\text{ThCr}_2\text{Si}_2$ -type compound  $\text{Dy}_2\text{O}_2\text{Te}$  is an antiferromagnet with  $T_N = 9.7$  K. A collinear  $A$ -type antiferromagnetic structure with the magnetic moment  $\mu = 9.4(1) \mu_B/\text{Dy}^{3+}$  at 3.5 K confined in the  $ab$  plane is identified directly from neutron diffraction experiments. Further research is called for on how the family of materials will evolve from antiferromagnetic  $\text{Dy}_2\text{O}_2\text{Te}$  to superconducting  $\text{Dy}_2\text{O}_2\text{Bi}$ . In external magnetic field, anomalous magnetic

properties including bifurcation between ZFC and FC magnetization, butterfly-shaped magnetic hysteresis, and slow magnetic relaxation could be induced in  $\text{Dy}_2\text{O}_2\text{Te}$ . These properties are directly associated with the field-induced metamagnetic transitions in  $\text{Dy}_2\text{O}_2\text{Te}$ . Our results of  $\text{Dy}_2\text{O}_2\text{Te}$  suggest that the rare-earth  $R_2\text{O}_2X$  ( $R$  = rare earth;  $X$  = Te, Bi, Sb) compounds are a promising material playground to further explore unconventional superconductivity and antiferromagnetism.

## ACKNOWLEDGMENTS

This work was supported by the National Natural Science Foundation of China (Grants No. 12074426, No. 11227906, No. 12104255, and No. 12004426), the National Key Research & Development Projects (Grants No. 2020YFA0406000 and No. 2020YFA0406003), and the Fundamental Research Funds for the Central Universities, and the Research Funds of Renmin University of China (Grants No. 22XNKJ40 and No. 21XNLG20).

- [1] F. Steglich, J. Aarts, C. D. Bredl, W. Lieke, D. Meschede, W. Franz, and H. Schäfer, *Phys. Rev. Lett.* **43**, 1892 (1979).
- [2] D. Jaccard, K. Behnia, and J. Sierro, *Phys. Lett. A* **163**, 475 (1992).
- [3] R. Movshovich, T. Graf, D. Mandrus, J. D. Thompson, J. L. Smith, and Z. Fisk, *Phys. Rev. B* **53**, 8241 (1996).
- [4] F. Grosche, S. Julian, N. Mathur, and G. Lonzarich, *Phys. B: Condens. Matter* **223-224**, 50 (1996).
- [5] T. T. M. Palstra, A. A. Menovsky, J. van den Berg, A. J. Dirkmaat, P. H. Kes, G. J. Nieuwenhuys, and J. A. Mydosh, *Phys. Rev. Lett.* **55**, 2727 (1985).
- [6] M. Rotter, M. Tegel, and D. Johrendt, *Phys. Rev. Lett.* **101**, 107006 (2008).
- [7] G. F. Chen, Z. Li, G. Li, W. Z. Hu, J. Dong, J. Zhou, X. D. Zhang, P. Zheng, N. L. Wang, and J. L. Luo, *Chin. Phys. Lett.* **25**, 3403 (2008).
- [8] K. Sasmal, B. Lv, B. Lorenz, A. M. Guloy, F. Chen, Y.-Y. Xue, and C.-W. Chu, *Phys. Rev. Lett.* **101**, 107007 (2008).
- [9] G. Wu, H. Chen, T. Wu, Y. L. Xie, Y. J. Yan, R. H. Liu, X. F. Wang, J. J. Ying, and X. H. Chen, *J. Phys.: Condens. Matter* **20**, 422201 (2008).
- [10] M. S. Torikachvili, S. L. Bud'ko, N. Ni, and P. C. Canfield, *Phys. Rev. Lett.* **101**, 057006 (2008).
- [11] J. Thompson, M. Nicklas, A. Bianchi, R. Movshovich, A. Llobet, W. Bao, A. Malinowski, M. Hundley, N. Moreno, P. Pagliuso, J. Sarrao, S. Nakatsuji, Z. Fisk, R. Borth, E. Lengyel, N. Oeschler, G. Sparn, and F. Steglich, *Phys. B: Condens. Matter* **329-333**, 446 (2003).
- [12] O. Stockert, J. Arndt, E. Faulhaber, C. Geibel, H. S. Jeevan, S. Kirchner, M. Loewenhaupt, K. Schmalzl, W. Schmidt, Q. Si, and F. Steglich, *Nat. Phys.* **7**, 119 (2011).
- [13] Q. Huang, Y. Qiu, W. Bao, M. A. Green, J. W. Lynn, Y. C. Gasparovic, T. Wu, G. Wu, and X. H. Chen, *Phys. Rev. Lett.* **101**, 257003 (2008).
- [14] J. Zhao, W. Ratchiff, J. W. Lynn, G. F. Chen, J. L. Luo, N. L. Wang, J. Hu, and P. Dai, *Phys. Rev. B* **78**, 140504(R) (2008).
- [15] A. I. Goldman, D. N. Argyriou, B. Ouladdiaf, T. Chatterji, A. Kreyssig, S. Nandi, N. Ni, S. L. Bud'ko, P. C. Canfield, and R. J. McQueeney, *Phys. Rev. B* **78**, 100506(R) (2008).
- [16] H. Chen, Y. Ren, Y. Qiu, W. Bao, R. H. Liu, G. Wu, T. Wu, Y. L. Xie, X. F. Wang, Q. Huang, and X. H. Chen, *Europhys. Lett.* **85**, 17006 (2009).
- [17] D. K. Pratt, W. Tian, A. Kreyssig, J. L. Zarestky, S. Nandi, N. Ni, S. L. Bud'ko, P. C. Canfield, A. I. Goldman, and R. J. McQueeney, *Phys. Rev. Lett.* **103**, 087001 (2009).
- [18] I. I. Mazin, D. J. Singh, M. D. Johannes, and M. H. Du, *Phys. Rev. Lett.* **101**, 057003 (2008).
- [19] P. Dai, J. Hu, and E. Dagotto, *Nat. Phys.* **8**, 709 (2012).
- [20] P. J. Hirschfeld, M. M. Korshunov, and I. I. Mazin, *Rep. Prog. Phys.* **74**, 124508 (2011).
- [21] W. Bao, *Chin. Phys. B* **22**, 087405 (2013).
- [22] A. Chubukov, *Annu. Rev. Condens. Matter Phys.* **3**, 57 (2012).
- [23] K. Ishida, Y. Nakai, and H. Hosono, *J. Phys. Soc. Jpn.* **78**, 062001 (2009).
- [24] F. A. Weber and T. Schleid, *Z. Anorg. Allg. Chem.* **625**, 1833 (1999).
- [25] J. Nuss and M. Jansen, *Z. Anorg. Allg. Chem.* **638**, 611 (2012).
- [26] J. Nuss and M. Jansen, *J. Alloys Compd.* **480**, 57 (2009).
- [27] H. Mizoguchi and H. Hosono, *J. Am. Chem. Soc.* **133**, 2394 (2011).
- [28] P. L. Wang, T. Kolodiazhnyi, J. Yao, and Y. Mozharivskyj, *Chem. Mater.* **25**, 699 (2013).
- [29] K. Matsumoto, H. Kawasoko, H. Kasai, E. Nishibori, and T. Fukumura, *Appl. Phys. Lett.* **116**, 191901 (2020).
- [30] H. Kim, C. J. Kang, K. Kim, J. H. Shim, and B. I. Min, *Phys. Rev. B* **93**, 125116 (2016).
- [31] H. Kim, C. J. Kang, K. Kim, J. H. Shim, and B. I. Min, *Phys. Rev. B* **91**, 165130 (2015).
- [32] L. Qiao, J. Chen, B. Lv, X. Yang, J. Wu, Y. Cui, H. Bai, M. Li, Y. Li, Z. Ren, J. Dai, and Z. Xu, *J. Alloys Compd.* **836**, 155229 (2020).
- [33] R. Sei, S. Kitani, T. Fukumura, H. Kawaji, and T. Hasegawa, *J. Am. Chem. Soc.* **138**, 11085 (2016).
- [34] K. Terakado, R. Sei, H. Kawasoko, T. Koretsune, D. Oka, T. Hasegawa, and T. Fukumura, *Inorg. Chem.* **57**, 10587 (2018).
- [35] R. Sei, H. Kawasoko, K. Matsumoto, M. Arimitsu, K. Terakado, D. Oka, S. Fukuda, N. Kimura, H. Kasai, E. Nishibori, K. Ohoyama, A. Hoshikawa, T. Ishigaki, T. Hasegawa, and T. Fukumura, *Dalton Trans.* **49**, 3321 (2020).
- [36] L. Qiao, N. Wu, T. Li, S. Wu, Z. Zhang, M. Li, J. Ma, B. Lv, Y. Li, C. Xu, Q. Tao, C. Cao, G. Cao, and Z. Xu, *Front. Phys.* **16**, 63501 (2021).
- [37] R. Sei, T. Fukumura, and T. Hasegawa, *ACS Appl. Mater. Interfaces* **7**, 24998 (2015).
- [38] J. Chappert, Y. Abbas, and J. Rossat-Mignod, *Physica B+C* **86-88**, 102 (1977).
- [39] D. Gatteschi and R. Sessoli, *Angew. Chem. Int. Ed.* **42**, 268 (2003).
- [40] H. Miyasaka, M. Julve, M. Yamashita, and R. Clérac, *Inorg. Chem.* **48**, 3420 (2009).
- [41] Y. Tian, W. Wang, Y. Chai, J. Cong, S. Shen, L. Yan, S. Wang, X. Han, and Y. Sun, *Phys. Rev. Lett.* **112**, 017202 (2014).
- [42] F. Shen, K. Pramanik, P. Brandão, Y. Zhang, N. C. Jana, X. Wang, and A. Panja, *Dalton Trans.* **49**, 14169 (2020).

- [43] N. Vernier and G. Bellessa, *J. Magn. Magn. Mater.* **177-181**, 962 (1998).
- [44] K. Matsuhira, Y. Hinatsu, and T. Sakakibara, *J. Phys.: Condens. Matter* **13**, L737 (2001).
- [45] B. G. Ueland, G. C. Lau, R. J. Cava, J. R. O'Brien, and P. Schiffer, *Phys. Rev. Lett.* **96**, 027216 (2006).
- [46] P. Cheng, H. Zhang, W. Bao, A. Schneidewind, P. Link, A. Grünwald, R. Georgii, L. Hao, and Y. Liu, *Nucl. Instrum. Methods Phys. Res. Sect. A* **821**, 17 (2016).
- [47] J. Rodríguez-Carvajal, *Phys. B* **192**, 55 (1993).
- [48] A. Le Bail, H. Duroy, and J. Fourquet, *Mater. Res. Bull.* **23**, 447 (1988).
- [49] See <http://www.mcphase.de>.
- [50] C. Tian, F. Pan, S. Xu, K. Ai, T. Xia, and P. Cheng, *Appl. Phys. Lett.* **116**, 202402 (2020).
- [51] J. Llanos, S. Conejeros, R. Cortés, V. Sánchez, P. Barahona, and O. Pena, *Mater. Res. Bull.* **43**, 312 (2008).
- [52] E. F. Bertaut, *Acta Cryst. A* **24**, 217 (1968).
- [53] G. Shirane, *Acta Cryst.* **12**, 282 (1959).
- [54] H. Kawasoko, K. Ohoyama, R. Sei, K. Matsumoto, D. Oka, A. Hoshikawa, T. Ishigaki, and T. Fukumura, *AIP Adv.* **9**, 115301 (2019).
- [55] K. Binder and A. P. Young, *Rev. Mod. Phys.* **58**, 801 (1986).
- [56] X. Li, J. Sheng, C. Tian, Y. Wang, T. Xia, L. Wang, F. Ye, W. Tian, J. Wang, J. Liu, H. Zhang, W. Bao, and P. Cheng, *Europhys. Lett.* **122**, 67006 (2018).
- [57] A. Maignan, V. Hardy, S. Hébert, M. Drillon, M. R. Lees, O. Petrenko, D. M. K. Paul, and D. Khomskii, *J. Mater. Chem.* **14**, 1231 (2004).
- [58] R. Schenker, M. N. Leuenberger, G. Chaboussant, D. Loss, and H. U. Güdel, *Phys. Rev. B* **72**, 184403 (2005).
- [59] D. A. Garanin, *Phys. Rev. B* **75**, 094409 (2007).
- [60] E. Rousset, M. Piccardo, M.-E. Boulon, R. W. Gable, A. Soncini, L. Sorace, and C. Boskovic, *Chem. Eur. J.* **24**, 14768 (2018).
- [61] J. Sheng, X. Li, C. Tian, J. Song, X. Li, G. Sun, T. Xia, J. Wang, J. Liu, D. Xu, H. Zhang, X. Tong, W. Luo, L. Wu, W. Bao, and P. Cheng, *Phys. Rev. B* **101**, 174516 (2020).